DETTACHED EDDY SIMULATION OF THE TRANSONIC FLOW OVER A CIRCULAR CYLINDER

Rafael Garcia Leal
University of Brasilia, Brasilia, DF, 70910-900, Brazil
der.jaguar@gmail.com

Roberto Francisco Bobenrieth Miserda
University of Brasilia, Brasilia, DF, 70910-900, Brazil
rfbm@unb.br

Abstract. *The objective of this work is the numerical simulation of the unsteady aerodynamic forces acting over a circular cylinder in transonic flow. The case studied is supercritical, with a fully turbulent boundary layer, where the Mach number is 0.8 and the Reynolds number is 500,000. The compressible Navier-Stokes equations are numerically solved using a finite volume discretization in combination with the skew-symmetric form of Ducros' fourth-order numerical scheme for the flux calculations, while the time marching process is achieved using a third-order Runge-Kutta scheme. For this case, a Detached Eddy Simulation is implemented, based on a variation proposed by Bender and Menter over the SST-DES formulation of Strelets. This numerical simulation is two-dimensional, due to the computational restrictions imposed by the high-density grid that is needed in order to capture the very complex and unsteady nature of the viscous-shock interactions that are characteristic of this type of flow. The mean numerical results are compared to experimental ones, and good agreement is found.*

Keywords*: Transonic Flow, Circular Cylinder, Detached Eddy Simulation, Viscous-Shock Interaction*

1. Introduction

The transonic cross flow over a circular cylinder is a very important subject in the field of unsteady aerodynamics due to its wide range of applications that includes, for example, the aerodynamics of missiles and aircrafts in transonic regime at high angles of attack. Despite the great importance of the matter, few works on the subject are available. The main reason for this is the very complex viscous-shock interaction that arises in this type of flow. This level of complexity is reflected in the level of difficulty imposed for experimental and numerical studies. Examples of experimental works in this subject are those of Welsh (1953), in which the experimental data for the cylinder have been acquired from flight tests instead of from wind tunnel tests, of Sreedhara Murty and Rose (1977), in which the vortex-shedding frequency, the mean surface friction and pressure coefficients distributions as well as the pressure drag over the cylinder have been measured and the work of Rodriguez (1984), in which the pressure distribution, unsteady lift and drag coefficients and the power spectra have been measured for compressible subsonic and transonic cross flows over a circular cylinder.

In this context, the numerical approach rises as an alternative for studying the problem. However, because of the intrinsic difficulties of the task, the great majority of the methodologies proposed to numerically study transonic cross-flows over a circular cylinder are based on the solution of the compressible Euler equations. Examples of such works are those of Pandolfi and Larocca (1989), in which the Euler equations are solved by means of a finite difference method based upon an upwind hybrid formulation exclusively for the transonic cylinder, of Hafez and Wahba (2004), in which the potential and stream functions, with entropy and vorticity corrections for transonic and supersonic flows are numerically solved for the case of the subsonic, transonic and supersonic cylinders and the work of French (2004), in which a conservative cell vertex with Lax-Wendroff time-stepping scheme is used to solve the Euler equations for Ni's two-dimensional channel and for the transonic cylinder.

With an Euler's equations based approach, it is not possible to capture the complex viscous-shock interactions that are characteristic of this type of flow. Ishii and Kuwahara (1984) solved the turbulent Navier-Stokes equations numerically, but due to the limitations of the MacCormack numerical method in combination with the Baldwin-Lomax turbulence model as well as the low grid density used, it was not possible to simulate a fully unsteady flow with viscous-shock interaction and only the vortex shedding was captured. The main objective of this work is to simulate the unsteady and complex topology associated with the viscous-shock interaction that arises in the transonic flow over a circular cylinder and to calculate the unsteady aerodynamic forces acting over it.

In order to achieve this objective, the compressible Navier-Stokes equations, with the Detached Eddy Simulation turbulence-closure model proposed by Strelets (2001), are solved. This is done using a finite volume approach, with fluxes calculated using the skew-symmetric form of Ducros' fourth-order numerical scheme (Ducros *et al*., 2000) while the time marching processes is achieved using a third-order Runge-Kutta scheme. The performed numerical simulation is two-dimensional, due to the computational restrictions imposed by the high-density grid that is needed in order to capture the very complex and unsteady nature of the viscous-shock interactions that are characteristic of this type of flow.

2. Methodology

The nondimensional form of the compressible Reynolds-averaged Navier-Stokes equations can be written as (Anderson, Tannehill and Pletcher, 1983):

$$\frac{\partial \overline{\rho}}{\partial t} + \frac{\partial}{\partial x_i}(\overline{\rho}\underline{u}_i) = 0 \tag{1}$$

$$\frac{\partial}{\partial t}(\overline{\rho}\underline{u}_i) + \frac{\partial}{\partial x_j}(\overline{\rho}\underline{u}_i\underline{u}_j) = -\frac{\partial \overline{p}}{\partial x_i} + \frac{\partial}{\partial x_j}\left[\left(\underline{\mu} + \mu_t\right)\underline{S}_{ij}\right] \tag{2}$$

$$\frac{\partial}{\partial t}\left[\overline{\rho}\left(\underline{e} + \frac{1}{2}\underline{u}_j^2\right)\right] + \frac{\partial}{\partial x_i}\left[\overline{\rho}\left(\underline{e} + \frac{1}{2}\underline{u}_j^2\right)\underline{u}_i\right] = -\frac{\partial}{\partial x_i}(\overline{p}\underline{u}_i) + \frac{\partial}{\partial x_i}\left(\underline{\mu}\,\underline{S}_{ij}\underline{u}_j\right) + \frac{\partial}{\partial x_i}\left[\left(\underline{k} + \gamma k_t\right)\left(\partial \underline{T}/\partial x_i\right)\right] \tag{3}$$

where the over bar indicates the Reynolds mean and the under bar refers to the Favre mean, or mass-averaged mean, defined as $\underline{f} = \overline{\rho f}/\overline{\rho}$. All the variables are in nondimensional form and have their usual meaning, i.e., x_i is the i-direction spatial coordinate, t is the temporal coordinate, ρ is the density, u_i is the i-direction component of the velocity vector, p is the pressure, μ is the dynamic viscosity, S_{ij} is the rate-of-strain tensor, e is the internal energy per unit of mass, T is the temperature, k is thermal conductivity and γ is the specific heat ratio. The subscript t indicates the turbulent properties. The nondimensional form of the flow variables and properties are defined as

$$\begin{gathered} x_i = \frac{x_i^*}{D^*}, \quad \underline{u}_i = \frac{\underline{u}_i^*}{U_\infty^*}, \quad t = \frac{t^*}{c^*/U_\infty^*}, \quad \overline{p} = \frac{\overline{p}^*}{\rho_\infty^*\left(U_\infty^*\right)^2}, \quad \overline{\rho} = \frac{\overline{\rho}^*}{\rho_\infty^*}, \quad \underline{\mu} = \frac{\underline{\mu}^*}{\mu_\infty^*}, \\ \underline{e} = \frac{\underline{e}^*}{\left(U_\infty^*\right)^2}, \quad c_v = \left[\frac{T_\infty^*}{\left(U_\infty^*\right)^2}\right]c_v^*, \quad \underline{T} = \frac{\underline{T}^*}{T_\infty^*}, \end{gathered} \tag{4}$$

where the asterisk denotes dimensional quantities and the subscript ∞ indicates the properties for the undisturbed flow. The nondimensional viscous-stress tensor is given by

$$\underline{S}_{ij} = \frac{1}{\mathrm{Re}}\left[\left(\frac{\partial \underline{u}_i}{\partial x_j} + \frac{\partial \underline{u}_j}{\partial x_i}\right) - \frac{2}{3}\delta_{ij}\frac{\partial \underline{u}_k}{\partial x_k}\right] \tag{5}$$

where the Reynolds number is defined as

$$\mathrm{Re} = \frac{\rho_\infty^* U_\infty^* L^*}{\mu_\infty^*}. \tag{6}$$

The Mach and the Prandtl numbers are respectively defined as

$$M = \frac{U_\infty^*}{\sqrt{\gamma R^* T_\infty^*}}, \qquad \mathrm{Pr} = \frac{c_p^*}{k_\infty^*}\mu_\infty^* \tag{7}$$

In this work, the Prandtl number is considered a constant with the value $\mathrm{Pr} = 0.72$. For a thermally and calorically perfect gas, the nondimensional equation of state can be written as

$$p = (\gamma - 1)\rho e \tag{8}$$

and

$$T = \frac{\gamma M^2 p}{\rho}. \tag{9}$$

The nondimensional molecular viscosity is obtained using Sutherland's formula

$$\underline{\mu} = C_1 \frac{\underline{T}^{3/2}}{\underline{T} + C_2}, \qquad C_1 = \left[\frac{\left(T_\infty^*\right)^{1/2}}{\mu_\infty^*} \right] C_1^*, \qquad C_2 = \frac{C_2^*}{T_\infty^*}, \tag{10}$$

where C_1 and C_2 are the nondimensional constants of the Sutherland's formula, with their dimensional counterparts represented by the asterisk. The nondimensional thermal conductivity is obtained as a function of the viscosity by

$$\underline{k} = \frac{\underline{\mu}}{(\gamma - 1) M^2 \,\mathrm{Re}\,\mathrm{Pr}}, \tag{11}$$

In order to close the system of equations defined by Eqs. (1), (2) and (3), the eddy viscosity, μ_t, and the eddy conductivity, k_t, must be modeled. In this work, the SST-DES formulation of Strelets *et al* (2001) is used. This DES formulation is based on the two-equation eddy-viscosity turbulence model proposed by Menter (1994), known as the Menter SST. In this model, the nondimensional transport equation for the turbulent kinetic energy, k, is given by

$$\frac{\partial}{\partial t}(\overline{\rho}\, k) + \frac{\partial}{\partial x_i}(\overline{\rho}\, \underline{u}_i\, k) = P_k - \beta^* \overline{\rho}\, \omega k + \frac{1}{\mathrm{Re}} \frac{\partial}{\partial x_i} \left[(\underline{\mu} + \mu_t \sigma_k) \frac{\partial k}{\partial x_i} \right], \tag{12}$$

and the nondimensional transport equation for the specific dissipation rate, ω, is

$$\frac{\partial}{\partial t}(\overline{\rho}\, \omega) + \frac{\partial}{\partial x_i}(\overline{\rho}\, \underline{u}_i\, \omega) = \gamma \left(\frac{\overline{\rho}}{\mu_t} \right) \mathrm{Re}\, P_k - \beta\, \overline{\rho}\, \omega^2 + \frac{1}{\mathrm{Re}} \frac{\partial}{\partial x_i} \left[(\underline{\mu} + \mu_t \sigma_\omega) \frac{\partial \omega}{\partial x_i} \right] + 2 \overline{\rho} (1 - F_1) \sigma_{\omega 2} \frac{1}{\omega} \frac{\partial k}{\partial x_i} \frac{\partial \omega}{\partial x_i}, \tag{13}$$

The nondimensional eddy viscosity and eddy conductivity needed for the closure of Eqs. (2) and (3), respectively, are given by

$$\underline{\mu}_t = \mathrm{Re}\, \overline{\rho} \frac{a_1 k}{\max(a_1 \omega, S F_2)}, \qquad \underline{k}_t = \frac{\underline{\mu}_t}{(1 - \gamma) \mathrm{M}_\infty^2 \,\mathrm{Pr}_t}. \tag{14}$$

In the above equation, $a_1 = 0{,}31$, $S = \left| S_{ij} \right|$ and the form of the function F_2 is

$$F_2 = \tanh\left(\arg_2^2 \right), \qquad \arg_2 = \max\left(2 \frac{\sqrt{k}}{\beta^* \omega y}; \frac{1}{\mathrm{Re}} \frac{500 \underline{\mu}}{y^2 \overline{\rho}\, \omega} \right), \tag{15}$$

where y is the nearest distance to the wall and the value of the coefficient β^* is 0.09.

The blended coefficients β, γ, σ_k and σ_ω that appear in the transport equations for k and ω are given in a similar way, resulting in

$$\beta = F_1 \beta_1 + (1 - F_1) \beta_2, \quad \gamma = F_1 \gamma_1 + (1 - F_1) \gamma_2, \quad \sigma_k = F_1 \sigma_{k1} + (1 - F_1) \sigma_{k2}, \quad \sigma_\omega = F_1 \sigma_{\omega 1} + (1 - F_1) \sigma_{\omega 2}, \tag{16}$$

where the fixed-value coefficients are

$$\begin{aligned} &\beta_1 = 0.0750, \quad \beta_2 = 0.0828, \quad \gamma_1 = 0.5532, \quad \gamma_2 = 0.4403, \\ &\sigma_{k1} = 0.8500, \quad \sigma_{k2} = 1.0000, \quad \sigma_{\omega 1} = 0.5000, \quad \sigma_{\omega 2} = 0.8560. \end{aligned} \tag{17}$$

The blending function F_1 is

$$F_1 = \tanh\left(\arg_1^4\right), \qquad \arg_1 = \min\left[\max\left(\frac{\sqrt{k}}{\beta^*\omega y}; \frac{1}{\mathrm{Re}}\frac{500\mu}{y^2\omega\overline{\rho}}\right); \frac{4\overline{\rho}\sigma_{\omega 2}k}{CD_{k\omega}y^2}\right], \tag{18}$$

where the cross-diffusion term in the above equation is

$$CD_{k\omega} = \max\left(2\overline{\rho}\,\sigma_{\omega 2}\frac{1}{\omega}\frac{\partial k}{\partial x_j}\frac{\partial \omega}{\partial x_j}; 1.0\mathrm{E}^{-10}\right). \tag{19}$$

Finally, the production term is given by

$$P_k = \left(\mu_t S_{ij} - \frac{2}{3}\overline{\rho}\,k\delta_{ij}\right)\frac{\partial u_i}{\partial x_j}. \tag{20}$$

The idea behind the SST-DES formulation of Strelets *et al*. (2001) is to switch from the SST model to a LES model when the predicted turbulent length, L_t, is larger than the local grid spacing, Δ. In this case, the length scale used to compute the dissipation rate in the transport equation for the turbulent kinetic energy is replaced by the grid spacing. According to this idea, the second term of the right-hand side of Eq. (12), given by $\beta^*\overline{\rho}\omega k$ is substituted by $\beta^*\overline{\rho}\omega k \cdot F_{DES}$, where the destruction function is

$$F_{DES} = \max\left(\frac{L_t}{C_{DES}\Delta}; 1\right), \qquad L_t = \frac{\sqrt{k}}{\beta^*\omega}, \tag{21}$$

and the value of C_{DES} is equal to 0.78. It is important to note that without this destruction function, in this work is not possible to obtain an unsteady solution for the case studied.

Bender and Menter (2004) proposed a modification of this SST-DES formulation in order to avoid grid-induced separations. The destruction function is modified as

$$F_{DES} = \max\left[\frac{L_t}{C_{DES}\Delta}(1 - F_2); 1\right]. \tag{22}$$

The boundary conditions at the wall of the circular cylinder are a no-slip condition for the velocity field, an adiabatic wall for the temperature field and a null gradient in the normal direction at the wall for the pressure field. In this work, the numerical methodology proposed by Bobenrieth Miserda and Mendonça (2005) is used in order to solve the system of equations represented by Eqs. (1), (2), (3), (12) and (13). It is based on a finite volume discretization, where the fluxes are calculated using the skew-symmetric form of Ducros' fourth-order numerical scheme (Ducros *et al*., 2000). The time-marching process is achieved using a third-order Runge-Kutta scheme proposed by Shu (Yee, 1997) and a pressure-based explicit dissipation (Jameson, 1981) is used since the numerical method is a centered one.

4. Results

For the case studied in this work, the Mach number is 0.80 and the Reynolds number is 500,000. This is a supercritical Reynolds number, associated to a fully turbulent boundary layer. The characteristic length is the diameter of the circular cylinder, D^*. The computational grid has an O-topology that extends up to more than $200\,D^*$ in the free-stream direction. The minimum normal distance from the cylinder surface to the centroid of the control volumes is $2{,}85\times10^{-4}D^*$. This value is achieved by clustering points in the radial direction close to the cylinder surface. The cylinder surface is discretized by 720 control volumes, and there are 630 control volumes in the normal direction. These definitions result in a problem with 453,600 control volumes and 2,721,600 degrees of freedom.

Figure 1 shows the intense viscous-shock interactions for two different instants. The variable plotted is the nondimensional magnitude of the temperature gradient. It is possible to visualize the high level of complexity and unsteadiness of the viscous-shock interactions that occur during and after the separation of the boundary layer. The first common feature for these two images is that the boundary-layer separation point is associated with lambda shocks of variable intensities and sizes. The second one is the presence of connecting shocks between vortices with opposed rotation direction, in the same manner as reported by Bobenrieth Miserda and Mendonça (2005). The third one is the

presence of local quasi-strait shocks that are orthogonal to local shear layers that are positioned in the recirculation region near the wall. After an intense viscous-shock interaction, a von Kármán vortex street is formed.

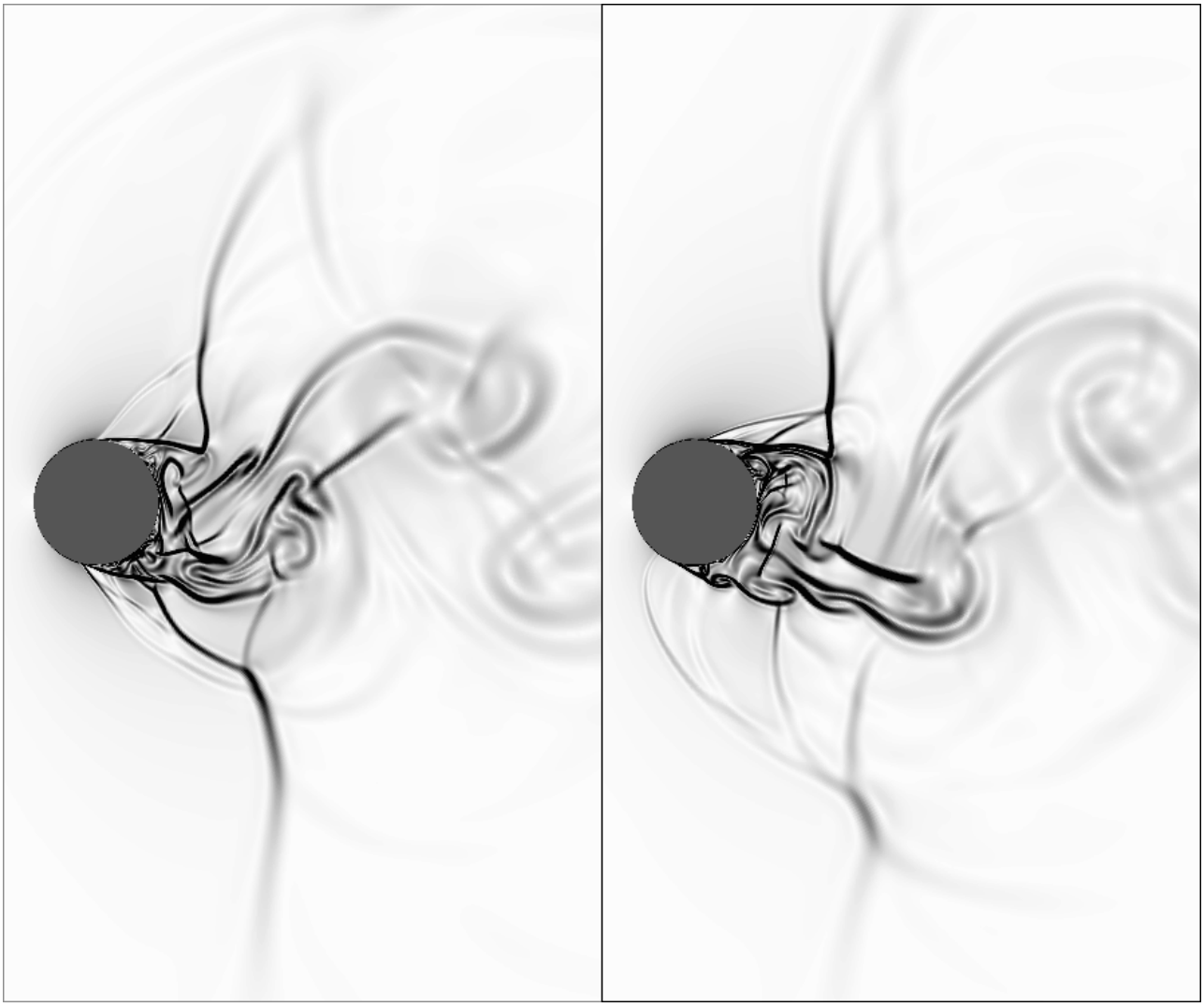

Figure 1. Viscous-shock interactions in the circular cylinder for $t = 136.76$ (left) and $t = 137.98$ (right). The variable plotted is the nondimensional magnitude of the temperature gradient. White corresponds to 0 and black corresponds to 3. The Mach number is 0.80 and the Reynolds numbers is 500,000.

Figure 2 presents the unsteady lift coefficient, C_L, and in a similar manner, Fig. (3) presents the unsteady drag coefficient, C_D. Comparing these two figures, it is possible to note a less chaotic behavior for the unsteady lift coefficient. It is also possible to note different characteristics frequencies for both cases. These features can be more precisely noted comparing Figs. 4 and 5, that presents the power spectrum, P_L and P_D, of the unsteady lift and drag coefficients as a function of the Strouhal number, S.

In Fig. 4, the computed power spectrum is more concentrated around its peak value that corresponds to a Strouhal number of 0.18, which is the same experimental value reported by Sreedhara Murty and Rose (1977) for the vortex-shedding frequency of this case. On the other hand, the power spectrum of the unsteady lift coefficient has a broader nature, with distinct peaks at the Strouhal numbers of 0.007, 0.086 and 0.13. This strongly suggest that the dominant frequency of the unsteady lift coefficient is closely related to the vortex-shedding frequency of the flow, and that the dominants frequencies of the unsteady drag coefficient are associated to the characteristics frequencies of the viscous-shock interactions, as can be seen in Fig. 1. This figure shows that, as one vortex is growing, very fast viscous-shock interactions are occurring.

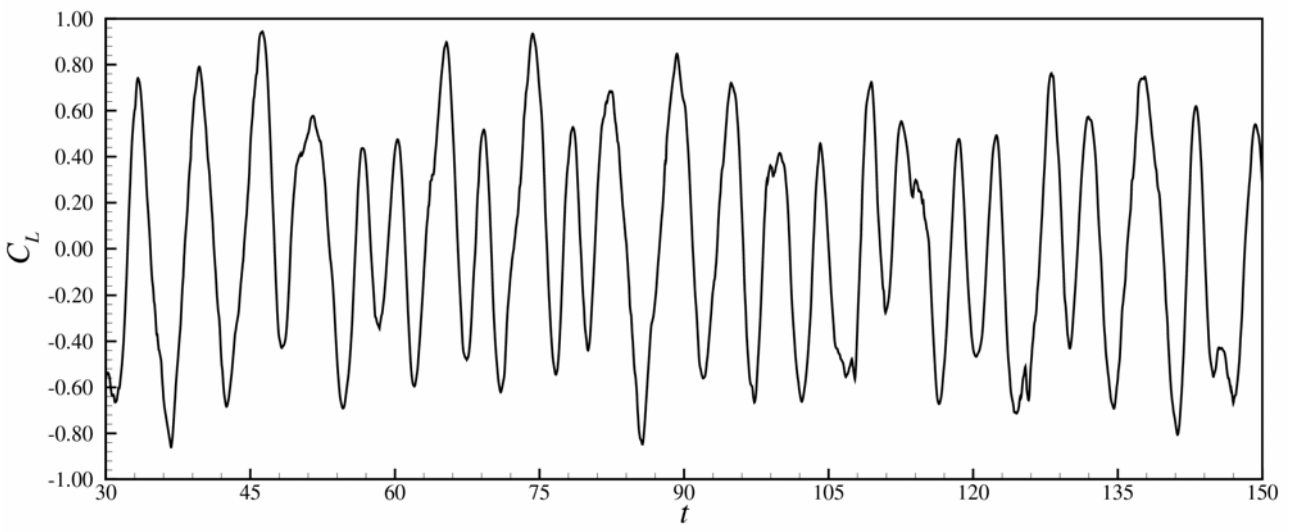

Figure 2. Unsteady lift coefficient as a function of time.

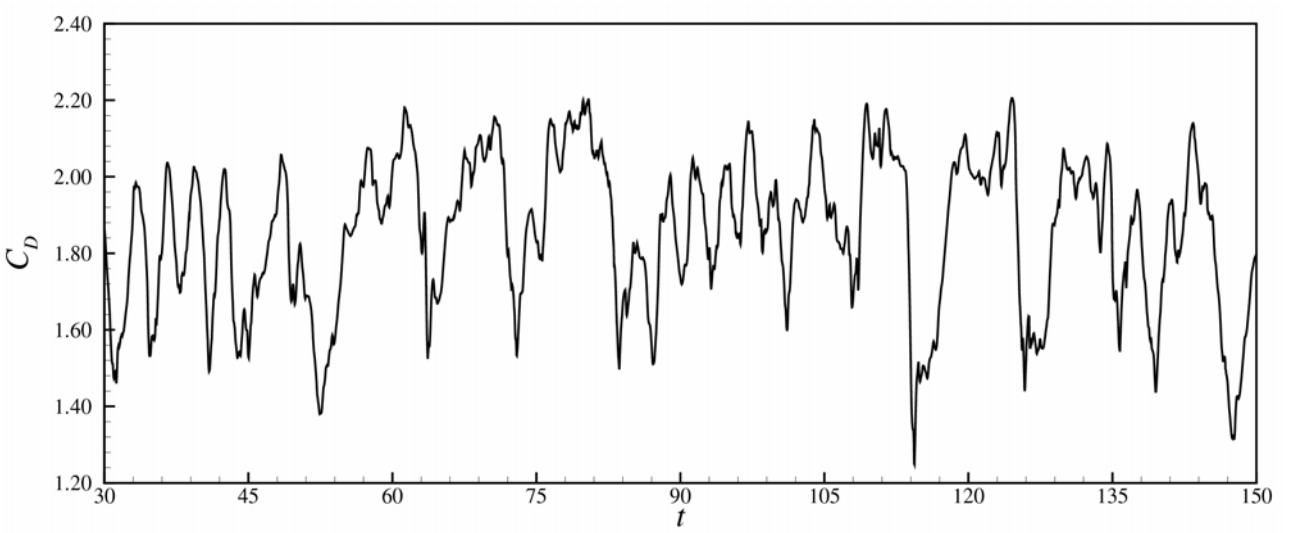

Figure 3. Unsteady drag coefficient as a function of time.

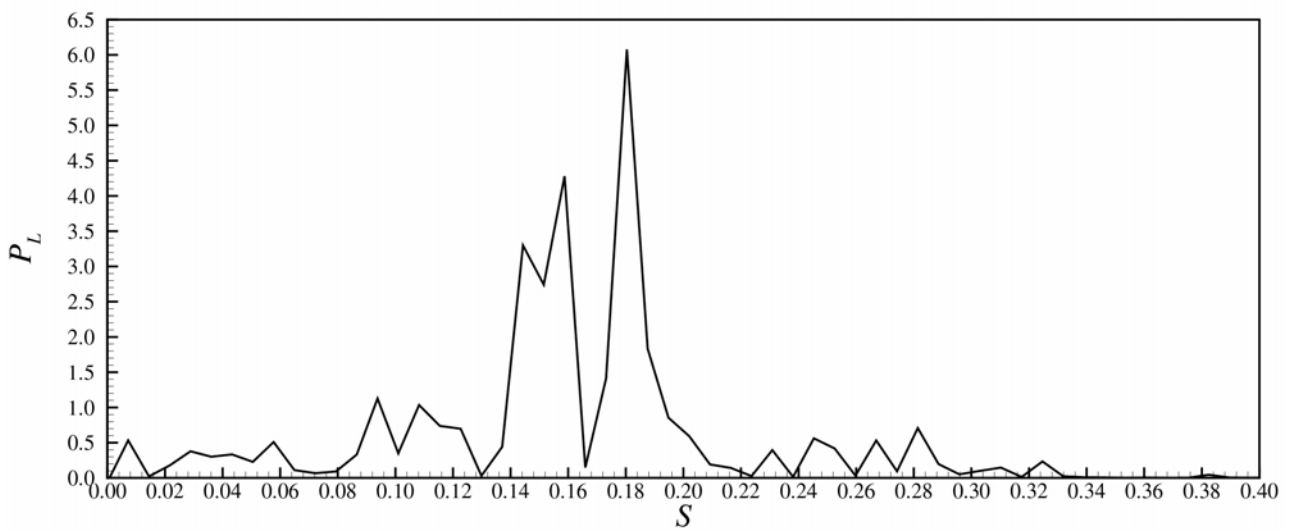

Figure 4. Power spectrum of the unsteady lift coefficient as a function of the Strouhal number.

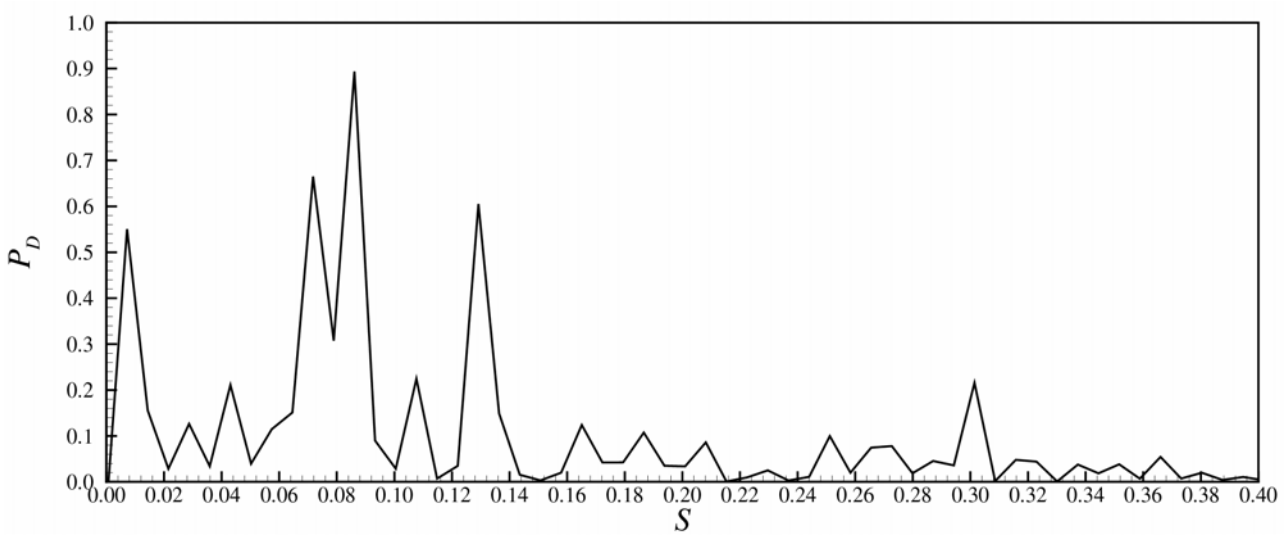

Figure 5. Power spectrum of the unsteady drag coefficient as a function of the Strouhal number.

Figure 6 compares the numerical and experimental data, obtained by Sreedhara Murty and Rose (1977), for the mean surface pressure coefficient, C_p. It can be observed that a very good agreement is observed up to the angle of 75°, approximately, that corresponds to the mean position of the boundary-layer separation point. This position is not captured precisely by the numerical simulation. One possible reason for this behavior could be an insufficient total time of simulation, due to the very chaotic nature of the flow. For grater values, the numerical results underestimate the value of this coefficient. This difference results in a variation of the value for the mean drag coefficient. The calculated value for this coefficient is 1.87 and the experimental value, reported by Sreedhara Murty and Rose (1977), is 1.5.

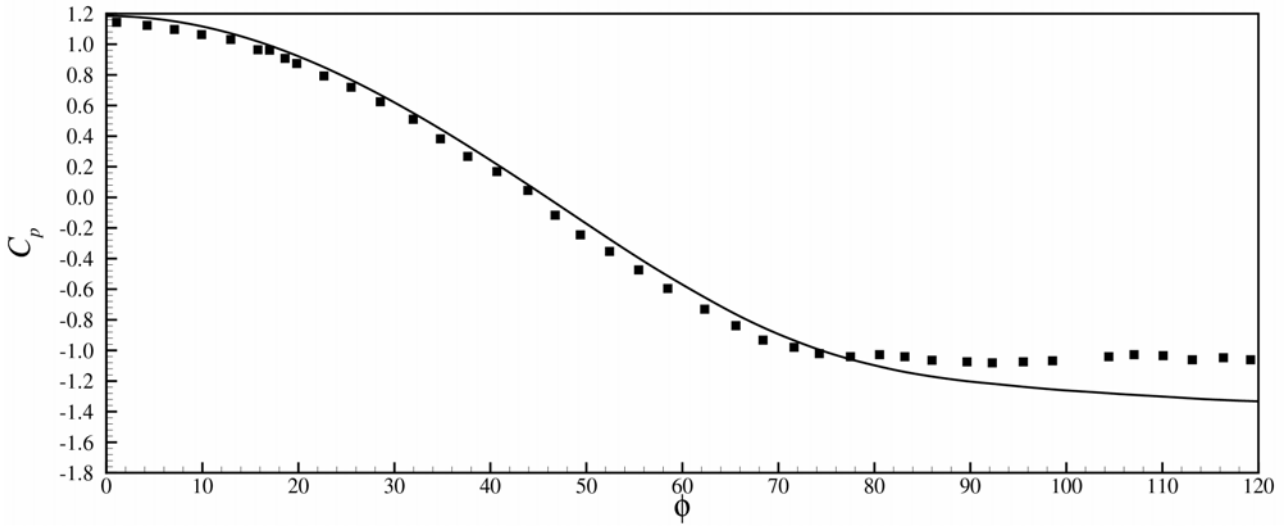

Figure 6. Surface pressure coeffcient. The variable plotted is the pressure coefficient over the circular cylinder surface, where the angle ϕ is measured from the frontal stagnation point. The continuous black line represents the numerical results and the black squares represent the experimental results of Sreedhara Murty and Rose.

5. Conclusions

A numerical methodology, based on the SST-DES formulation, is proposed in order to simulate the complex viscous-shock interactions that arise in the transonic flow over a circular cylinder. The performed numerical simulation is two-dimensional, due to the computational restrictions imposed by the high level of grid refinement that is necessary in order to capture the unsteady nature of the flow. The numerical results shows that a variety of complex viscous-shock interactions, such as lambda shocks associated with the boundary layer separation point, quasi-strait shocks that are normal to shear layers and connecting shock between vortices, occurs simultaneously, but not necessarily at the same

frequency, with the vortex-shedding of the flow. The results also show that the dominant frequency of the unsteady lift coefficient is closely associated with the vortex-shedding frequency. A very good agreement is found between the numerical and experimental values for this frequency. On the other hand, the power spectrum of the unsteady drag coefficient is broader, including high frequencies compared with the vortex shedding. This broader power spectrum is associated with the above mentioned viscous-shock interactions. The calculated mean drag coefficient is 24.7 % higher than the experimental one.

6. Acknowledgements

For carrying out the present work, the author has received financial support from CNPq (Conselho Nacional de Desenvolvimento Científico e Tecnológico), a Brazilian government entity aimed at promoting the scientific and technologic development.

7. References

Anderson, D. A., Tanehill, J. C., Pletcher, R., 1984, "Computational Fluid Mechanics and Heat Transfer", Hemisphere Publishing Corporation, New York.

Bender, R., Menter, F. R., 2002, "Experimental and Numerical Study of Reactive Flows in Complex Geometries with Relevance to Industrial Safety for Explosion Protection". 5th Framework Programme 1998-2002, Otterfing, Germany.

Bobenrieth Miserda, R. F., Mendonça, A. F. de, 2005, "Numerical Simulation of the Vortex-Shock Interactions in a Near-Base Laminar Flow", AIAA 43rd Aerospace Sciences Meeting and Exhibit, AIAA 2005-0316, Reno, Nevada.

Ducros, F., Ferrand, V., Nicoud, F., Weber, C., Darraq, D., Gacherieu, C., Poinsot, T., 1999, "Large-Eddy Simulation of the Shock/Turbulence Interaction," Journal of Computational Physics, Vol. 152, 1999, pp. 517, 549.

Ducros, F., Laporte, F., Soulères, T., Guinot, V., Moinat, P. and Caruelle, B., 2000, "High-Order Fluxes for Conservative Skew-Symmetric-like Schemes in Structured Meshes: Application to Compressible Flows," Journal of Computational Physics, Vol. 161, pp. 114, 139.

French, A. D., 2004, "Solution of the Euler Equations on Cartesian Grids", Applied Numerical Mathematics 49 (2004), pp. 367-379. Elsevier B. V.

Hafez, M., Wahba, E, 2004, "Inviscid Flows over a Cylinder", Comput. Methods Appl. Mech. Engrg. 193 (2004) pp. 1981-1995, Elsevier B. V.

Ishii, K., Kuwahara, K., 1984, "Computation of Compressible Flow Around a Circular Cylinder", AIAA 17th Fluid, Plasma Dynamics and Laser Conference, AIAA-84-1631, Snowmass, Colorado.

Jameson, A., Schmidt, W. and Turkel, E.,1981,"Numerical Solutions of the Euler Equations by Finite Volume Methods Using Runge-Kutta Time-Stepping Schemes," AIAA 14th Fluid and Plasma Dynamics Conference, AIAA-81-1259, Palo Alto, California.

Menter, F. R.,1994, "Two Equations Eddy Viscosity Turbulence Models for Engineering Applications", AIAA Journal, Vol. 32, N° 8.

Pandolfi, M., Larocca, F., 1989, "Transonic Flow about a Circular Cylinder", Computer & Fluids, Vol. 17, N° 1, pp. 205-220, Great Britain.

Rodriguez, O., 1984, "The Circular Cylinder in Subsonic and Transonic Flow", AIAA Journal, Vol. 22, N° 12, pp. 1713, 1718.

Sreedhara Murthy, V., Rose, W.C.,1977, "Form Drag, Skin Friction and Vortex Shedding Frequencies for Subsonic and Transonic Cross Flows on Circular Cylinder", AIAA 10th Fluid and Plasmadynamics Conference, AIAA- 77-687, Albuquerque, New Mexico.

Strelets, M., 2001, "Detached Eddy Simulation of Massively Separated Flows", 39th AIAA Aerospace Sciences Meeting and Exhibit, AIAA 2001-0879, Reno, Nevada.

Welsh, C. J., 1953, "The Drag of Finite Length Cylinders Determined from Flight Tests at High Reynolds Numbers for a Mach Number Range from 0.5 to 1.3", NACA TN 2941.

Yee, H. C.,1997,"Explicit and Implicit Multidimensional Compact High-Resolution Shock-Capturing Methods: Formulation," Journal of Computational Physics, Vol. 131, pp. 216, 232.

8. Responsibility notice

The authors are the only responsible for the printed material included in this paper.